Stability and electronic structure of Cu_2ZnSnS_4 surfaces: First-principles study

Peng Xu,[1] Shiyou Chen,[1,2] Bing Huang,[3] H. J. Xiang,[1] Xin-Gao Gong,[1] and Su-Huai Wei[3]

[1]*Key Laboratory for Computational Physical Sciences (MOE), State Key Laboratory of Surface Physics and Department of Physics, Fudan University, Shanghai 200433, China*

[2]*Key Laboratory of Polar Materials and Devices (MOE), East China Normal University, Shanghai 200241, China*

[3]*National Renewable Energy Laboratory, Golden, Colorado 80401, USA*

(Received 24 April 2013; published 17 July 2013)

Currently little is known about the atomic and electronic structure of Cu_2ZnSnS_4 (CZTS) surfaces, although the efficiency of kesterite-based solar cells has been increased to over 11%. Through the first-principles calculations, we studied the possible surface structures of the frequently observed cation-terminated (112) and anion-terminated $(\bar{1}\bar{1}\bar{2})$ surfaces, and found that the polar surfaces are stabilized by the charge-compensating defects, such as vacancies (V_{Cu}, V_{Zn}), antisites (Zn_{Cu}, Zn_{Sn}, Sn_{Zn}), and defect clusters ($Cu_{Zn} + Cu_{Sn}$, $2Zn_{Cu} + V_{Sn}$). In stoichiometric single-phase CZTS samples, Cu-enriched defects are favored on (112) surfaces and Cu-depleted defects are favored on $(\bar{1}\bar{1}\bar{2})$ surfaces, while in non-stoichiometric samples grown under Cu poor and Zn rich conditions both surfaces favor the Cu-depleted defects, which explains the observed Cu deficiency on the surfaces of the synthesized CZTS thin films. The electronic structure analysis shows that Cu-enriched surfaces produce detrimental states in the band gap, while Cu-depleted surfaces produce no gap states and are thus benign to the solar cell performance. The calculated surface properties are consistent with experimental observation that Cu-poor and Zn-rich CZTS solar cells have higher efficiency.

DOI: 10.1103/PhysRevB.88.045427 PACS number(s): 61.50.Ah, 68.35.B−, 68.47.Fg, 71.20.Nr

I. INTRODUCTION

The kesterite-structured Cu_2ZnSnS_4 (CZTS) and $Cu_2ZnSnSe_4$ (CZTSe) semiconductors have been intensively studied as candidate light-absorber materials for thin film solar cells and great progress has been made during the past few years.[1–7] Relative to the well-known solar cell absorber materials such as binary CdTe and ternary $Cu(In,Ga)Se_2$ (CIGSe), quaternary CZTS and CZTSe have drawn increasing attention because they not only possess the electronic and optical properties similar to CdTe and CIGSe (band gaps around 1.0–1.5 eV, high absorption coefficient, etc.),[8] but also have all component elements being nontoxic and earth abundant. This shows the advantages of the quaternary semiconductors with increased flexibility in the material properties. However, the increased number of elements also causes many properties to be complicated. For example, although the kesterite structure of CZTS can be derived from the binary zinc-blende and ternary chalcopyrite structures, there are many more types of possible lattice defects in quaternary CZTS.[9–11] Similar to the defect properties, the surface properties of CZTS also become more complicated, i.e., there are many possible structural patterns (surface defects) which have not yet been studied.

Surface properties of semiconductors have important influence on their photovoltaic performance, because the separation of the photogenerated electron-hole pairs happens usually near the surfaces or interfaces. A benign band bending near the surfaces may enhance the separation of electron-hole pair, while detrimental surface states deep in the band gap may act as recombination centers. Considering that most of the synthesized CZTS and CZTSe samples are thin films or nanocrystals,[12–15] which have high surface/volume ratios, the influence of surfaces on their photovoltaic performance is crucial. Although the CZTS and CZTSe based solar cells have achieved an energy efficiency as high as 11%,[7] the current knowledge about the surface properties is limited. For ternary $CuInSe_2$ (CISe), theoretical calculations[16,17] and experiments[18,19] showed that the formation of charge-compensating defects (V_{Cu}, Cu_{In}, In_{Cu}) stabilizes the polar (112)/$(\bar{1}\bar{1}\bar{2})$ surfaces relative to the nonpolar (110)/$(\bar{1}\bar{1}0)$ surfaces. Whether similar effects exist for quaternary CZTS has now become a natural question. Interestingly, XRD patterns of CZTS thin films showed that the most preferred surface orientation is (112)/$(\bar{1}\bar{1}\bar{2})$[20–23] rather than (110)/$(\bar{1}\bar{1}0)$. As there are much more intrinsic defects in CZTS than in CISe,[9–11] it is so far not clear what kind of surface defects stabilize the CZTS (112)/$(\bar{1}\bar{1}\bar{2})$ surfaces, and whether these surface defects produce detrimental states in the band gap.

One of the unique properties for CZTS is that the achievable chemical potential range for stable stochiometric CZTS is very narrow.[9–11] Therefore, to avoid bulk detrimental defects,[11] the synthesized samples are usually nonstoichiometric, e.g., the highest-efficiency solar cells are Cu poor and Zn rich with the element ratios $Cu/(Zn + Sn) \approx 0.8$ and $Zn/Sn \approx 1.2$, significantly deviating from their stoichiometric values.[24–26] The surfaces in the stoichiometric and nonstoichiometric samples can differ significantly, so understanding the surface differences might be the key to increasing the efficiency of the nonstoichiometric solar cells. A recent x-ray photoelectron (XPS) study found that the CZTS thin film has Cu-deficient surfaces[27] which may produce a downward band bending near the surface; however, the exact origin of the Cu deficiency and whether the surface Cu deficiency is a general character of CZTS samples are not clear.

All these open questions highlight the necessity of a computational study on the atomic and electronic structure of CZTS surfaces. In this paper, using the first-principle calculations we studied the energetic stability and the electronic structures of possible structure configurations for the experimentally preferred CZTS (112) and $(\bar{1}\bar{1}\bar{2})$ surfaces. Through the

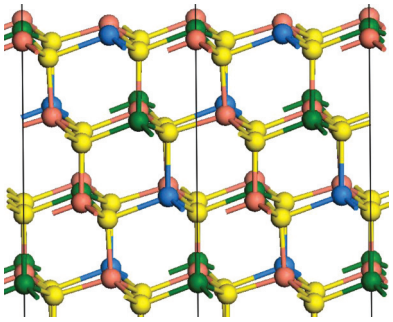

FIG. 1. (Color online) Structural plot of the cation-terminated (112) [top] and anion-terminated $(\bar{1}\bar{1}\bar{2})$ [bottom] surfaces of the kesterite CZTS. The red, green, blue, and yellow balls show Cu, Zn, Sn, and S atoms in order, and the black lines show the range of the surface unit cells. A (2×1) surface supercell is shown here.

calculation of the surface energies, we revealed the origin of the Cu deficiency, and discussed its dependence on the growth environment (chemical potentials). The electronic structure shows that Cu-enriched surfaces produce detrimental gap states, while Cu-deficient surfaces are clean surfaces without gap states and are beneficial to the solar cell performance, which can be facilitated by the Cu-poor and Zn-rich growth condition.

II. CONFIGURATIONS OF SURFACE STRUCTURE

The present study concentrates on the $(112)/(\bar{1}\bar{1}\bar{2})$ surfaces which are observed in XRD patterns.[20–23] The $(112)/(\bar{1}\bar{1}\bar{2})$ orientation of the chalcopyrite CISe and kesterite CZTS is equivalent to the $(111)/(\bar{1}\bar{1}\bar{1})$ of the binary zinc-blende structure, with the cation layer and anion layer stacked alternately as shown in Fig. 1. Therefore, the ideal $(112)/(\bar{1}\bar{1}\bar{2})$ surfaces without reconstruction belong to Tasker's type-III polar surfaces,[28] i.e., two surfaces terminated with a cation layer and an anion layer exhibit charge imbalance, which leads to long-range charge transfer or otherwise electrostatic catastrophe, so usually the polar surfaces are not stable. The polar surfaces can be stabilized when the surface reconstructs, such as forming vacancies or adsorbing atoms that can compensate the charge imbalance. An empirical electron counting rule (ECR) was proposed,[29–31] which states that a surface is stable when the cation dangling bonds at the surface are unoccupied and the anion dangling bonds at the surface are fully occupied. The ECR is applicable to many semiconductor surfaces such as those of GaAs,[32] ZnO,[33] and CISe,[17] e.g., the $(112)/(\bar{1}\bar{1}\bar{2})$ surfaces of CISe with the ECR satisfied through the formation of surface defects (Cu vacancy, Cu on In antisite, etc.) were found to be stable both theoretically[16,17] and experimentally.[18,19] Therefore, in the present study of the CZTS $(112)/(\bar{1}\bar{1}\bar{2})$ surfaces, we use ECR to screen and classify the possible structure configurations.

For the cation-terminated (112) surface, there are two Cu, one Zn, and one Sn dangling bonds on each (1×1) surface unit cell as shown in Fig. 1; each dangling bond has 1/4, 1/2, and 1 electron, respectively, so two extra electrons per cell should be removed to satisfy the ECR. This can be achieved through the formation of acceptorlike surface defects. Based on the ECR, we considered all possible configurations of the surface defects in (1×1) or (2×1) surface supercells, and low energy configurations under different chemical potential conditions are shown in Figs. 2(a)–2(g), where the top and bottom panels show the configurations before and after structural relaxation, respectively: (a) the two extra electrons are compensated by two Cu vacancies ($2V_{Cu}$) in the (1×1) unit cell; (b) one Zn vacancy (V_{Zn}) in (1×1) cell; (c) the four extra electrons are compensated by one Sn vacancy (V_{Sn}) in the (2×1) supercell; (d) one Zn-on-Sn antisite (Zn_{Sn}) in (1×1) cell; (e) one Zn vacancy and two Cu vacancies ($V_{Zn} + 2V_{Cu}$) in (2×1) cell. (f) Two Zn-on-Cu antisites and one Sn vacancy ($2Zn_{Cu} + V_{Sn}$) in (1×1) cell; (g) one Cu-on-Zn and one Cu-on–Sn antisite ($Cu_{Zn} + Cu_{Sn}$) in (2×1) cell.

The formation of these charge-compensating surface defects induces large structural relaxation from the ideal structure, similar to that on the surfaces of binary and ternary semiconductors,[17,34–36] i.e., most of the top-layer cations tend to move inward to the surface and form sp^2 bond angle. Specifically, (a) for $2V_{Cu}$, the relaxation is mainly perpendicular to the surface (along z direction); the Zn and Sn move downward by about 0.69 Å and 0.89 Å. (b) For V_{Zn}, the three nearest-neighbor S atoms in the subsurface layer displace towards the vacancy by about 0.25 Å, 0.08 Å, and 0.44 Å, respectively. Additionally, the top-layer Sn atom moves downward by about 0.87 Å in the z direction. (c) For V_{Sn}, the right Sn atom on the surface moves upward by about 0.6 Å, making it obviously out of the plane. (d) For Zn_{Sn}, the top two layers become almost coplanar. (e) For $V_{Zn} + 2V_{Cu}$, the rest Cu, Zn, and Sn atoms move downward by about 0.73 Å, 0.71 Å, and 0.84 Å, respectively. (f) For $2Zn_{Cu} + V_{Sn}$, the Zn atom plane move downward by about 0.66 Å. (g) For $Cu_{Zn} + Cu_{Sn}$, the movement along the z direction is −0.66 Å, −0.64 Å, and +0.60 Å for Cu, Zn, and Sn on the top layer in order. This large relaxation makes the top two layers get close to being coplanar, except for the Sn atom.

For the $(\bar{1}\bar{1}\bar{2})$ surface terminated with the S anions (bottom surface in Fig. 1), two electrons should be added per (1×1) surface unit cell to satisfy the ECR. This can be achieved through the formation of donorlike surface defects. Figures 2(h)–2(k) shows four lowest-energy configurations with different surface defects: (h) Sn adatom (Sn_{adatom}) in (2×1) cell; (i) two Zn-on-Cu antisite ($2Zn_{Cu}$) in (1×1) cell; (j) Sn-on-Zn antisite (Sn_{Zn}) in (1×1) cell; (k) Zn adatom (Zn_{adatom}) in (1×1) cell. Note that the cation-on-cation antisite defects are in the subsurface layer. Structural relaxation shows that (h) for Sn_{adatom}, the adatom on the bridging site is more stable than on top of the S atom by about 93 meV/a_0^2 (the calculated lattice constant $a_0 = 5.33$ Å). (i) For $2Zn_{Cu}$, due to the larger size of Zn than Cu, the S on the topmost surface move away from the antisite defect by a maximum of 0.17 Å. (j) For Sn_{Zn}, the three nearest neighbor S atoms on the surface displace away from Sn_{Zn} by more than 0.1 Å due to the larger atomic size of Sn relative to Zn. (k) For Zn_{adatom}, the adatom is also more stable at the bridging site, with a large displacement from on top of the S atom. Besides the structures shown in Figs. 2(h)–2(k), the higher-energy structures such as two 2Cu adatoms ($2Cu_{adatom}$) and S vacancy (V_S) are considered but not shown here.

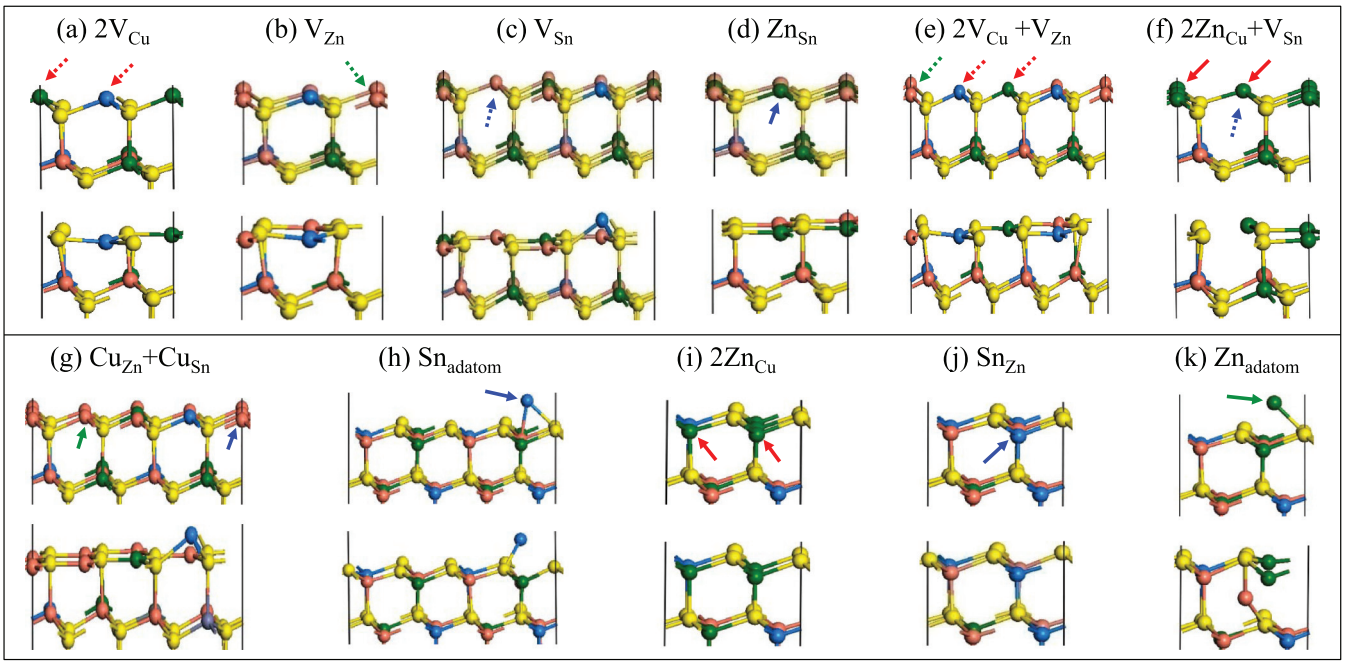

FIG. 2. (Color online) Sideview of the kesterite CZTS (112) [(a)–(g)] and $(\bar{1}\bar{1}\bar{2})$ [(h)–(k)] surfaces with different structure configurations (surface defects). The top and bottom parts of each panel show the structures before and after relaxation, respectively. The red, green, blue, and yellow balls show Cu, Zn, Sn, and S atoms in order. The arrows denote the location of the surface defects, and the dashed line means that one atom is removed from the site.

III. CALCULATION PROCEDURE OF (112)/$(\bar{1}\bar{1}\bar{2})$ SURFACE ENERGIES

Usually the theoretical study of surfaces uses the slab model, in which the sum of the surface energies of the top (t) and bottom (b) surfaces, $E_s^t + E_s^b$, can be calculated by

$$E_s^t + E_s^b = E_{\text{slab}} - N E_{\text{bulk}}(\text{CZTS}) + n_{\text{Cu}}\left(\mu_{\text{Cu}} + E_{\text{Cu}}^{\text{bulk}}\right) + n_{\text{Zn}}\left(\mu_{\text{Zn}} + E_{\text{Zn}}^{\text{bulk}}\right) + n_{\text{Sn}}\left(\mu_{\text{Sn}} + E_{\text{Sn}}^{\text{bulk}}\right) + n_S\left(\mu_S + E_S^{\text{bulk}}\right), \quad (1)$$

where E_{slab} is the calculated total energy of the slab, E_{bulk}(CZTS) is the total energy per unit cell of the bulk CZTS, N is the number of CZTS unit cells that the ideal slab model contains,n_{Cu} (similarly for n_{Zn}, n_{Sn}, and n_{S}) is the number of Cu atom removed from the ideal slab to the external reservoir during the formation of a certain surface or surface defect, and $\mu_{\text{Cu}} + E_{\text{Cu}}^{\text{bulk}}$ gives the energy of Cu in the chemical reservoir (similarly for Zn, Sn, and S). In the expression $\mu_{\text{Cu}} + E_{\text{Cu}}^{\text{bulk}}$, μ_{Cu} is the chemical potential of Cu referenced to bulk Cu and $E_{\text{Cu}}^{\text{bulk}}$ is the total energy per atom of the bulk Cu, so $\mu_{\text{Cu}} = 0$ means that Cu is as rich as in the growth environment that the bulk Cu will start to form. To synthesize the single-phase CZTS samples without the coexistence of bulk Cu, Zn, Sn, and S, and secondary compounds such as CuS, Cu_2S, SnS, SnS_2, ZnS, and Cu_2SnS_3, the chemical potentials μ_{Cu}, μ_{Zn}, μ_{Sn}, and μ_{S} are limited in a range shown in Fig. 3, which is similar to previous results from the calculation using the generalized gradient approximation (GGA).[9]

For some surfaces, like (110) or (001), a symmetrical slab with equivalent top and bottom surfaces can be constructed, so the surface energy of an individual surface can be calculated directly from $(E_s^t + E_s^b)/2$. However, for the (112) surface terminated with cations [similarly for $(\bar{1}\bar{1}\bar{2})$ surface terminated with anions], it is impossible to construct a slab with the equivalent top and bottom surfaces, so the direct method given above cannot give the top and bottom surface energy separately.

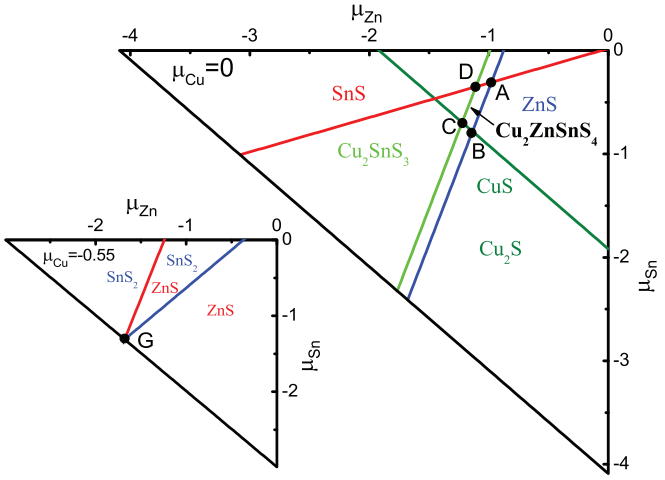

FIG. 3. (Color online) Calculated region in the (μ_{Cu}, μ_{Zn}, μ_{Sn}, μ_{S}) chemical potential space that stabilizes the single phase of Cu_2ZnSnS_4, as shown by the area surrounded by four corners A-B-C-D in $\mu_{\text{Cu}} = 0$ (Cu-rich) plane and the point G in the $\mu_{\text{Cu}} = -0.55$ eV (Cu poor) plane. μ_{Cu}, μ_{Zn}, μ_{Sn}, and μ_{S} are in the unit of eV. The stable region shrinks as Cu become poorer (decreasing μ_{Cu}). Two points E (−0.15,−1.30,−0.81,−0.42) and F (−0.35,−1.40,−0.83,−0.29) are on the line of A-G.

In order to calculate the surface energy for the (112) and $(\bar{1}\bar{1}\bar{2})$ surfaces individually, we used an algorithm similar to that proposed in Ref. 37, in which the (111) and $(\bar{1}\bar{1}\bar{1})$ surface energies of zinc-blende structures are calculated through a three-step procedure. Specifically, to calculate the surface energy of the cation-terminated (112) surface of CZTS, first we construct a symmetrical slab with the cation-terminated (001) surfaces as top and bottom surfaces, so the surface energy of the cation-terminated (001) can be calculated according to Eq. (1). Note here the polar (001) surface is passivated by the pseudohydrogen atoms, and the contribution of pseudohydrogen atoms will be cancelled in the final results. Then, we construct a wedge with two anion-terminated $(\bar{1}\bar{1}\bar{2})$ surfaces and one cation-terminated (001) surface (all the three surfaces are passivated by pseudohydrogen), and the surface energy of the anion-terminated $(\bar{1}\bar{1}\bar{2})$ surfaces can be calculated from the difference between the energy of all the surfaces of the wedge and the energy of one cation-terminated (001) surface. Finally, we construct an asymmetrical slab with the cation-terminated (112) as the top surface (not passivated by pseudohydrogen, but by surface defects) and the anion-terminated $(\bar{1}\bar{1}\bar{2})$ as the bottom surface (passivated by pseudohydrogen as in the wedge), so the absolute surface energy of the cation-terminated (112) surface with a certain structural configuration (surface defect) can be calculated. A similar calculation procedure also works for the $(\bar{1}\bar{1}\bar{2})$ surface. An example is given in the Supplemental Material[43] for the calculation procedure in detail.

The total energy and electronic structure calculations of the slabs and wedges are performed using the plane wave method with projector augmented wave (PAW) pseudopotentials[38,39] as implemented in the VASP code.[40,41] The cutoff energy for the plane wave basis is 500 eV, as required by the pseudohydrogen pseudopotentials. The local-density approximation (LDA)[42] to the exchange-correlation functional is used for the structural relaxation and total energy calculation with the force on every atom converged to lower than 0.05 eV/Å. The pseudohydrogen surface passivation makes the charge of each surface atom satisfy the octet rule, i.e., a $q = 1.75e$, $q = 1.5e$, $q = 1e$, and $q = 0.5e$ charged pseudohydrogen is added to passivate the Cu, Zn, Sn, and S dangling bond, respectively, as plotted in the Supplemental Material.[43] For asymmetrical slabs, the remaining polarity after passivation may produce error in the total energy and potential due to the finite size of the slabs; the dipole correction is applied as described in the Ref. 44. The electronic structure of the slabs, such as the projected density of states (PDOS) on different layers of the slab, is calculated using the nonlocal hybrid functional HSE06,[45–47] which has been shown to be more accurate in calculating the band gap and electronic structure of CZTS.[48,49] The k meshes used for the static HSE06 calculation are $2 \times 2 \times 1$ for (1×1) unit cell and $1 \times 2 \times 1$ for (2×1) unit cell slabs.

IV. STABILITY OF DIFFERENT (112)/$(\bar{1}\bar{1}\bar{2})$ SURFACE

With the surface energy calculated for different structure configurations (surface defects), we can now analyze the stability of different configurations. This will be discussed for two kinds of CZTS samples: (i) the stoichiometric samples synthesized under the chemical potential conditions that favor the single-phase CZTS, like the points A, B, C, D, E, F, and G points shown in Fig. 3; (ii) nonstoichiometric samples synthesized under the chemical potential conditions going out of the stable region, e.g., Cu poor and Zn rich samples with Cu/(Zn + Sn) ratios lower than 1 and Zn/Sn ratios higher than 1.

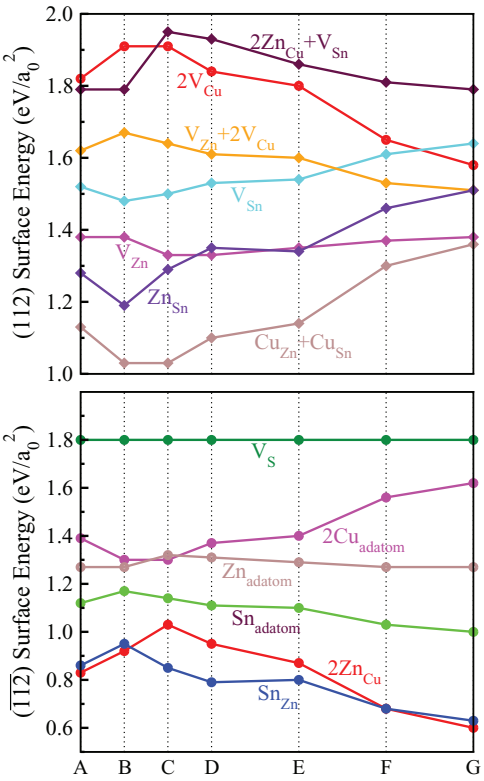

FIG. 4. (Color online) Surface energies (in eV/a_0^2) of different structure configurations as a function of the chemical potential along the A-B-C-D-E-F-G line, for the kesterite CZTS (112) and $(\bar{1}\bar{1}\bar{2})$ surfaces.

Surfaces of stoichiometric samples. Figure 4 shows the calculated surface energies of possible structure configurations of CZTS (112) and $(\bar{1}\bar{1}\bar{2})$ surfaces, under the chemical potential conditions along the A-B-C-D-E-F-G line. For the cation-terminated (112) surface, the acceptorlike defects are formed as shown in Figs. 2(a)–2(g), among which Cu enriched defect pair $Cu_{Zn} + Cu_{Sn}$ is energetically the most favorable surface defect in the whole chemical region. The other two surface defects V_{Zn} and Zn_{Sn} have slightly higher energy (at about 1.3 eV/a_0^2) than that of $Cu_{Zn} + Cu_{Sn}$ (at about 1.1 eV/a_0^2). However, the difference is not very large, so all three defects are expected to form on the (112) surfaces with the popularity of the $Cu_{Zn} + Cu_{Sn}$ configuration slightly higher than the other two. As a result of these three dominated defects, the (112) surfaces are relatively Cu richer and Zn, Sn poorer than inside the bulk of the stoichiometric CZTS samples.

On the anion-terminated $(\bar{1}\bar{1}\bar{2})$ surfaces, the donorlike defects are formed, among which Sn_{Zn} and $2Zn_{Cu}$ in the subsurface layer have the comparable energy (0.8 eV/a_0^2), obviously lower than other defects [Fig. 4(b)]. For the $(\bar{1}\bar{1}\bar{2})$ surfaces of the chalcopyrite CISe, the dominant defect is In_{Cu}[17]

which is similar to Sn_{Zn} and $2Zn_{Cu}$ on compensating the charge of the anion-terminated surfaces. The comparable energy of Sn_{Zn} and $2Zn_{Cu}$ indicates that the number of low-energy configurations increases for the $(\bar{1}\bar{1}\bar{2})$ surfaces of CZTS, and both kinds of surface configurations may exist, which makes the surface properties more complicated. In contrast to the case of the (112) surface, the formation of Sn_{Zn} and $2Zn_{Cu}$ makes the $(\bar{1}\bar{1}\bar{2})$ surface Cu poorer and Zn, Sn richer than inside the bulk.

Comparing the absolute surface energy values of (112) and $(\bar{1}\bar{1}\bar{2})$ low-energy configurations, we can see that the $(\bar{1}\bar{1}\bar{2})$ value is always lower than the corresponding (112) value, indicating that the popularity of the anion-terminated $(\bar{1}\bar{1}\bar{2})$ surfaces should be higher than the cation-terminated (112) surfaces. When the Cu chemical potential is 0 (the Cu richest conditions, like at the B and C points in Fig. 3), the popularity of the $(\bar{1}\bar{1}\bar{2})$ surfaces is slightly higher than (112) surfaces, and under all other conditions (Cu becomes poorer), the popularity difference becomes more obvious. Experimentally, the (112)/$(\bar{1}\bar{1}\bar{2})$ orientation preference is observed for the synthesized thin films;[20–23] however, it is not clear whether the surface is the cation terminated (112) or the anion terminated $(\bar{1}\bar{1}\bar{2})$. Our calculation shows clearly that the anion-terminated $(\bar{1}\bar{1}\bar{2})$ surfaces should be easier to form for the free-standing stoichiometric samples. On the other hand, since the cation-terminated (112) surfaces prefer Cu-rich defects while the anion-terminated $(\bar{1}\bar{1}\bar{2})$ surfaces prefer Cu-poor defects, the higher popularity of the $(\bar{1}\bar{1}\bar{2})$ surfaces means that overall the surfaces of the stoichiometric samples should be Cu poor, and Zn, Sn rich, which is consistent with the recent x-ray photoelectron (XPS) observation that the CZTS thin film has Cu-deficient surfaces.[27]

Surfaces of nonstoichiometric samples. Under the real growth conditions to optimize the material properties,[11] the chemical potential is often not exactly in the range that stabilizes the single-phase stochiometric CZTS, so the synthesized samples are usually nonstoichiometric. One interesting observation of the CZTS solar cells is that the highest efficiency is achieved when the light-absorber material CZTS is Cu poor and Zn rich, with the element ratios $Cu/(Zn+Sn) \approx 0.8$ and $Zn/Sn \approx 1.2$ significantly deviating from the ideal values,[24–26] so it is important to investigate the surface properties in these nonstoichiometric thin films.

Figure 5 shows the (112) and $(\bar{1}\bar{1}\bar{2})$ surface energies of CZTS when the chemical potential goes beyond the stable range. Several trends can be found. (i) When Cu is rich (μ_{Cu} close to 0), the Cu-enriched $Cu_{Zn}+Cu_{Sn}$ is the dominant (112) surface defect, but as Cu becomes poorer, $2V_{Cu}$ becomes dominant, and $V_{Zn}+2V_{Cu}$ and $2Zn_{Cu}+V_{Sn}$ also decrease their energies significantly. This means that the most popular structures of (112) surfaces in Cu-poor samples is $2V_{Cu}$, different from in stoichiometric samples. (ii) The low-energy

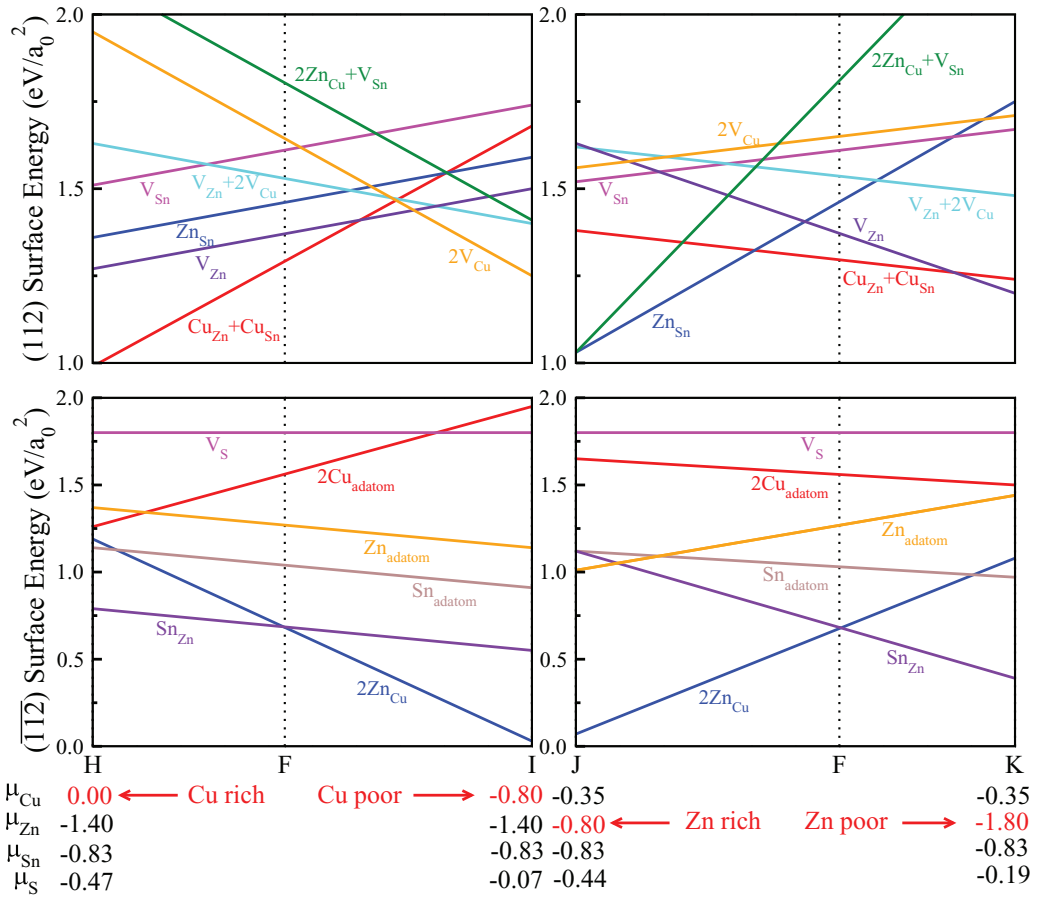

FIG. 5. (Color online) (112) and $(\bar{1}\bar{1}\bar{2})$ surface energy versus the chemical potentials: μ_{Cu} (left) and μ_{Zn} (right). The chemical potential conditions H-F-I and J-F-K are chosen to be in the vicinity of the regions that stabilize the single-phase CZTS in Fig. 3.

defects of $(\bar{1}\bar{1}2)$ surfaces are always Sn_{Zn} and $2Zn_{Cu}$, in the whole range of μ_{Cu}, and the energy of $2Zn_{Cu}$ decreases rapidly as Cu becomes poor, indicating that the $(\bar{1}\bar{1}2)$ surfaces become even more Cu poor in the Cu-poor nonstoichiometric CZTS samples. (iii) As Zn becomes rich (μ_{Zn} increases), the (112) surfaces are dominated by Zn_{Sn} and $2Zn_{Cu}+V_{Sn}$, and $(\bar{1}\bar{1}2)$ surfaces are dominated by $2Zn_{Cu}$, so both surfaces are Zn rich and Cu poor. (iv) As Zn becomes poor, the (112) surfaces are dominated by V_{Zn} and $Cu_{Zn}+Cu_{Sn}$, and $(\bar{1}\bar{1}2)$ surfaces are dominated by Sn_{Zn}, making both surfaces Zn poor and Cu rich. In short, when the growth condition changes from Cu rich, Zn poor to Cu poor, Zn rich, (112) surfaces reconstruct from $Cu_{Zn}+Cu_{Sn}$ or V_{Zn} to $2V_{Cu}$, $V_{Zn}+2V_{Cu}$, $2Zn_{Cu}+V_{Sn}$ or Zn_{Sn}, and $(\bar{1}\bar{1}2)$ surfaces may reconstruct from Sn_{Zn} to $2Zn_{Cu}$. A similar change of the preferred surface defects also exists in CISe,[17] i.e., from the Cu rich to Cu poor conditions, the stable defect changes from Cu-enriched Cu_{In} to Cu-depleted $2V_{Cu}$ on (112) surfaces.

Based on the above analysis, we predict that the CZTS films with $Cu/(Zn+Sn)\approx 0.8$ and $Zn/Sn\approx 1.2$ should have $2V_{Cu}$, $2Zn_{Cu}+V_{Sn}$, or Zn_{Sn} dominated (112) surfaces and $2Zn_{Cu}$ dominated $(\bar{1}\bar{1}2)$ surfaces. The calculated surface energies reveal quantitatively the origin of the observed Cu deficiency. Furthermore, in the Cu poor and Zn rich thin films, the energy of the stable $(\bar{1}\bar{1}2)$ surface configurations becomes much lower than that of (112) surfaces, indicating the anion-terminated $(\bar{1}\bar{1}2)$ surfaces should have much higher popularity than the (112) surfaces, so their contribution to photovoltaic performance should be more important.

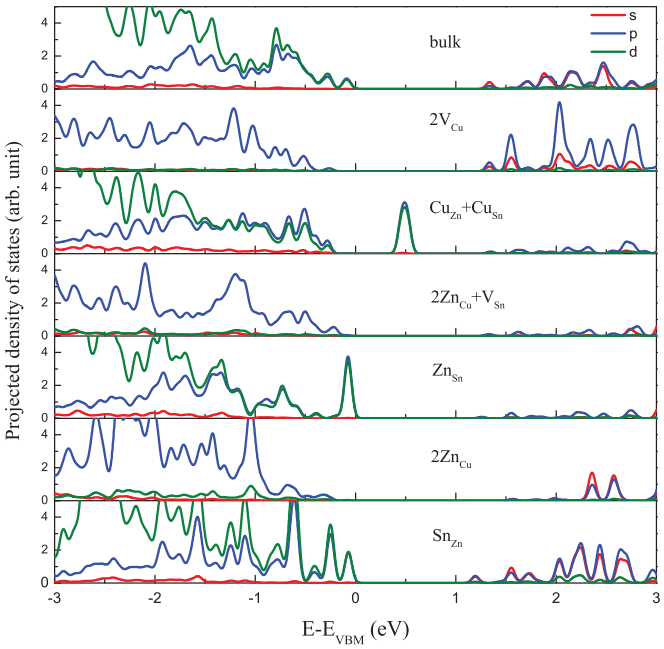

FIG. 6. (Color online) Partial density of states (PDOS) projected on different bilayers of the slabs with different surface defects. The calculation is performed using the HSE06 hybrid functional. The PDOS of the bilayers in the middle of the slab is taken as the DOS of bulk CZTS. (Note that due to the finite size and k-point sampling, this could introduce some errors in the details of the shape of the DOS peaks, but the band edge shift induced by surfaces can be correctly described.)

V. ELECTRONIC STRUCTURE OF LOW-ENERGY SURFACES

The surface energy calculations have revealed the dominant structure configurations, and we now discuss the electronic structure consequences of these configurations, to investigate their influence on the CZTS solar cell performance.

Figure 6 shows the partial density of states (PDOS) projected on different bilayers (cation + anion) of the slabs. The PDOS of the surface bilayers for different surface configurations [$2V_{Cu}$, $Cu_{Zn}+Cu_{Sn}$, $2Zn_{Cu}+V_{Sn}$, Zn_{Sn} for (112) surfaces, and $2Zn_{Cu}$, Sn_{Zn} for $(\bar{1}\bar{1}2)$ surfaces] is aligned with the valence band maximum (VBM) level of the bulk PDOS taken as the reference. It is clear that there is a band gap around 1.3 eV in the bulk PDOS. (Note, because the HSE06 hybrid functional is only used to calculate the DOS whereas the relaxation of both the lattice constants and atomic coordinates uses the LDA functional to reduce the computational cost, the gap is slightly smaller than the value 1.5 eV calculated previously where the HSE06 functional was used for the relaxation of the atomic coordinates at the experimental lattice constants.[48]) If the surface states fall deep inside the band gap of the bulk, they may become the recombination centers of the photo-generated electron-hole pairs on the surfaces, which will be detrimental to the solar cell efficiency.

Comparing the PDOS of different surface configurations, we find that (i) all the charge-compensated surfaces do not induce valence band edge upshift. Like in the bulk CZTS, the top of the valence band is mainly composed of the S $3p$ and Cu $3d$ states, whose p-d hybridization is much stronger than that with the Zn $3d$ or Sn $4d$ states at the top of the valence band, so only the Cu related defects ($2V_{Cu}$, $Cu_{Zn}+Cu_{Sn}$, $2Zn_{Cu}+V_{Sn}$, $2Zn_{Cu}$) may induce a valence band edge shift. For $2V_{Cu}$, $2Zn_{Cu}+V_{Sn}$ and $2Zn_{Cu}$ surface configurations, there is no Cu cation on the surface bilayers, so the PDOS near the valence band edge is actually decreased, although the band edge is only slightly shifted down due to the p-d hybridization between surface S and the subsurface Cu. The case of $Cu_{Zn}+Cu_{Sn}$ is different and will be discussed later.

(ii) All the Cu-depleted and Zn-enriched surface defects do not induce conduction band edge downshift, and thus produce no states in the gap. Furthermore, the conduction band edge of $2Zn_{Cu}$ surface is even pushed up, and thus the electrons may be repelled from the surfaces, decreasing the possibility of the electron-hole recombination. Based on this, we can predict the existence of Cu-depleted and Zn-enriched surfaces is benign to the solar cell performance.

(iii) In contrast to the Cu-depleted and Zn-enriched ones, the Cu-enriched or Zn-depleted surface defects can create deep levels inside the bulk band gap, e.g., one electronic energy level of $Cu_{Zn}+Cu_{Sn}$ is in the middle of the band gap of bulk CZTS, and that of Sn_{Zn} is below the conduction band edge of the bulk. From the PDOS of $Cu_{Zn}+Cu_{Sn}$, we can see that the surface states in the gap inherit the p-d character of the valence band edge states, which can be understood by considering that both Cu_{Zn} and Cu_{Sn} are acceptor defects and the replacement of Zn or Sn by Cu enhances the p-d repulsion in the valence band, so the unoccupied states introduced by $Cu_{Zn}+Cu_{Sn}$ are pushed up significantly from the valence

band into the gap, and thus become the conduction band edge. These surface-induced localized gap states are detrimental to the solar cell performance, because they act as recombination centers and trap the photogenerated electrons as well as reduce the effective band gap, thus the open circuit voltage V_{OC}. Fortunately, our surface energy calculations have shown that the thin films grown under Cu-poor and Zn-rich conditions can significantly reduce such kinds of detrimental surface states, which gives another explanation for the observed high efficiency of solar cells with Cu poor and Zn rich absorbers.[24–26] Since the (112) surfaces with $Cu_{Zn} + Cu_{Sn}$ defects can possibly form in stoichiometric samples, we can expect that the solar cells based on stoichiometric absorbers should have limited efficiency, consistent with experimental observations.[11]

VI. CONCLUSIONS

Using the first-principles calculations, we have determined the stable structures of the kesterite CZTS(112)/$(\bar{1}\bar{1}\bar{2})$ surfaces with a series of charge-compensating defects. Two different growth conditions (chemical potentials) are considered. Under the growth condition that favors stoichiometric CZTS samples, the cation-terminated (112) surfaces prefer to form Cu-enriched defects and the anion-terminated $(\bar{1}\bar{1}\bar{2})$ surfaces prefer to form Cu-depleted defects. However, under the Cu-poor and Zn-rich condition that favors nonstoichiometric samples, both surfaces prefer to form Cu-depleted defects. Through the electronic structure analysis, we found that Cu-enriched surfaces produce detrimental states in the band gap while Cu-depleted surfaces are clean without deep gap states, which provides an explanation to the observation that Cu-poor and Zn-rich conditions are beneficial to the solar cell efficiency.

ACKNOWLEDGMENTS

S.H.W. would like to thank Glenn Teeter and Ingrid Repins for helpful discussions. The work at Fudan University was partially supported by the Special Funds for Major State Basic Research, National Natural Science Foundation of China (NSFC), International collaboration project, and Program for Professor of Special Appointment (Eastern Scholar). Computation was performed in the Supercomputer Center of Fudan University. S.C. is supported by NSFC under Grants No. 61106087, No. 10934002, and No. 91233121. The work at NREL was funded by the US Department of Energy (DOE), under Contract No. DE-AC36-08GO28308.

[1] A. Weber, S. Schmidt, D. Abou-Ras, P. Schubert-Bischoff, I. Denks, R. Mainz, and H. W. Schock, Appl. Phys. Lett. **95**, 041904 (2009).
[2] C. Steinhagen, M. G. Panthani, V. Akhavan, B. Goodfellow, B. Koo, and B. A. Korgel, J. Am. Chem. Soc. **131**, 12554 (2009).
[3] A. Redinger and S. Siebentritt, Appl. Phys. Lett. **97**, 092111 (2010).
[4] A. Redinger, D. M. Berg, P. J. Dale, and S. Siebentritt, J. Am. Chem. Soc. **133**, 3320 (2011).
[5] C. M. Fella, A. R. Uhl, Y. E. Romanyuk, and A. N. Tiwari, Phys. Status Solidi A **209**, 1043 (2012).
[6] M. Grossberg, J. Krustok, J. Raudoja, and T. Raadik, Appl. Phys. Lett. **101**, 102102 (2012).
[7] T. K. Todorov, J. Tang, S. Bag, O. Gunawan, T. Gokmen, Y. Zhu, and D. B. Mitzi, Adv. Energy Mater. **3**, 34 (2013).
[8] J. P. Leitão, N. M. Santos, P. A. Fernandes, P. M. P. Salomé, A. F. da Cunha, J. C. González, and F. M. Matinaga, Thin Solid Films **519**, 7390 (2011).
[9] S. Chen, J.-H. Yang, X. G. Gong, A. Walsh, and S.-H. Wei, Phys. Rev. B **81**, 245204 (2010).
[10] S. Chen, X. G. Gong, A. Walsh, and S. H. Wei, Appl. Phys. Lett. **96**, 021902 (2010).
[11] S. Chen, A. Walsh, X. G. Gong, and S. H. Wei, Adv. Mater. **25**, 1522 (2013).
[12] T. Tanaka, D. Kawasaki, M. Nishio, Q. Guo, and H. Ogawa, Phys. Status Solidi C **3**, 2844 (2006).
[13] K. Tanaka, M. Oonuki, N. Moritake, and H. Uchiki, Sol. Energy Mater. Sol. Cells **93**, 583 (2009).
[14] S. C. Riha, B. A. Parkinson, and A. L. Prieto, J. Am. Chem. Soc. **131**, 12054 (2009).
[15] M. Pal, N. R. Mathews, R. S. Gonzalez, and X. Mathew, Thin Solid Films **535**, 78 (2013).
[16] J. E. Jaffe and A. Zunger, Phys. Rev. B **64**, 241304 (2001).
[17] S. B. Zhang and S.-H. Wei, Phys. Rev. B **65**, 081402 (2002).
[18] S. Siebentritt, N. Papathanasiou, J. Albert, and M. C. Lux-Steiner, Appl. Phys. Lett. **88**, 151919 (2006).
[19] A. Hofmann and C. Pettenkofer, Surf. Sci. **606**, 1180 (2012).
[20] P. A. Fernandes, P. M. P. Salomé, and A. F. da Cunha, Thin Solid Films **517**, 2519 (2009).
[21] H. Yoo and J. Kim, Thin Solid Films **518**, 6567 (2010).
[22] A. V. Moholkar, S. S. Shinde, A. R. Babar, K.-U. Sim, Y.-b. Kwon, K. Y. Rajpure, P. S. Patil, C. H. Bhosale, and J. H. Kim, Solar Energy **85**, 1354 (2011).
[23] J. He, L. Sun, K. Zhang, W. Wang, J. Jiang, Y. Chen, P. Yang, and J. Chu, Appl. Surf. Sci. **264**, 133 (2013).
[24] T. K. Todorov, K. B. Reuter, and D. B. Mitzi, Adv. Mater. **22**, E156 (2010).
[25] D. B. Mitzi, O. Gunawan, T. K. Todorov, K. Wang, and S. Guha, Sol. Energy Mater. Sol. Cells **95**, 1421 (2011).
[26] B. Shin, O. Gunawan, Y. Zhu, N. A. Bojarczuk, S. J. Chey, and S. Guha, Prog. Photovolt: Res. Appl. **21**, 72 (2013).
[27] M. Bör, B.-A. Schubert, B. Marsen, S. Krause, S. Pookpanratana, T. Unold, L. Weinhardt, C. Heske, and H.-W. Schock, Appl. Phys. Lett. **99**, 112103 (2011).
[28] P. W. Tasker, J. Phys. C: Solid State Phys. **12**, 4977 (1979).
[29] M. D. Pashley, Phys. Rev. B **40**, 10481 (1989).
[30] D. J. Chadi, J. Vac. Sci. Technol. A **5**, 834 (1987).
[31] W. A. Harrison, J. Vac. Sci. Technol. **16**, 1492 (1979).
[32] N. Moll, A. Kley, E. Pehlke, and M. Scheffler, Phys. Rev. B **54**, 8844 (1996).
[33] O. Dulub, U. Diebold, and G. Kresse, Phys. Rev. Lett. **90**, 016102 (2003).
[34] J. E. Northrup and S. Froyen, Phys. Rev. B **50**, 2015 (1994).
[35] A. Ohtake, J. Nakamura, T. Komura, T. Hanada, T. Yao, H. Kuramochi, and M. Ozeki, Phys. Rev. B **64**, 045318 (2001).
[36] B. Meyer and D. Marx, Phys. Rev. B **67**, 035403 (2003).

[37]S. B. Zhang and S.-H. Wei, Phys. Rev. Lett. **92**, 086102 (2004).
[38]P. E. Blöchl, Phys. Rev. B **50**, 17953 (1994).
[39]G. Kresse and D. Joubert, Phys. Rev. B **59**, 1758 (1999).
[40]G. Kresse and J. Hafner, Phys. Rev. B **47**, 558 (1993).
[41]G. Kresse and J. Furthmüller, Phys. Rev. B **54**, 11169 (1996).
[42]W. Kohn and L. J. Sham, Phys. Rev. **140**, A1133 (1965).
[43]See Supplemental Material at http://link.aps.org/supplemental/10.1103/PhysRevB.88.045427 for an example on which the calculation procedure is introduced in detail.
[44]G. Makov and M. C. Payne, Phys. Rev. B **51**, 4014 (1995).
[45]J. Heyd, G. E. Scuseria, and M. Ernzerhof, J. Chem. Phys. **118**, 8207 (2003).
[46]J. Jaramillo, G. E. Scuseria, and M. Ernzerhof, J. Chem. Phys. **118**, 1068 (2003).
[47]J. Paier, M. Marsman, K. Hummer, G. Kresse, I. C. Gerber, and J. G. Ángyaán, J. Chem. Phys. **124**, 154709 (2006).
[48]S. Chen, X. G. Gong, A. Walsh, and S.-H. Wei, Appl. Phys. Lett. **94**, 041903 (2009).
[49]S. Botti, D. Kammerlander, and M. A. L. Marques, Appl. Phys. Lett. **98**, 241915 (2011).